

# We are IntechOpen, the world's leading publisher of Open Access books Built by scientists, for scientists

6,900

Open access books available

185,000

International authors and editors

200M

Downloads

Our authors are among the

154

Countries delivered to

TOP 1%

most cited scientists

12.2%

Contributors from top 500 universities



WEB OF SCIENCE™

Selection of our books indexed in the Book Citation Index  
in Web of Science™ Core Collection (BKCI)

Interested in publishing with us?  
Contact [book.department@intechopen.com](mailto:book.department@intechopen.com)

Numbers displayed above are based on latest data collected.  
For more information visit [www.intechopen.com](http://www.intechopen.com)



---

# Stability of $\gamma$ -UMo Nuclear Fuel Alloys by Thermal Analysis

---

Fábio Branco Vaz de Oliveira and  
Delvonei Alves de Andrade

Additional information is available at the end of the chapter

<http://dx.doi.org/10.5772/53340>

---

## 1. Introduction

The development of a nuclear fuel for research reactor applications must take into account the non-proliferation of nuclear grade materials for weapons requirements, according to the Reduced Enrichment of Research and Test Reactors (RERTR) program. To minimize a potential problem with the use of high enriched fuels, i.e., the production of Pu and its possible utilization in nuclear weapons, several reactors have been converted their fuels from high to low enrichment. It is now acceptable a level of less than 20% of  $U^{235}$ .

However, to compensate for the resultant loss of power, fuel densities must be raised and, thus, a new class of fuels, mainly the metallic ones, is under development. Those fuels are replacing the current oxides and silicides, and the most promising candidate has emerged from the binary system U-Mo, gamma phase stabilized, according firstly to the confirmation of its good behavior under fabrication and irradiation conditions, observed in several “in pile” tests performed over the years [1]. Compositions of 7 and 10 wt. % molybdenum are considered to be the most promising for the gamma-stabilized uranium fuels.

$\gamma$ UMo fuels can be used in two main configurations in fuel plates. If mixed as metallic powder in aluminum powder matrix, they are called dispersion fuels. The other way, a foil of  $\gamma$ UMo is co-rolled with the aluminium cladding to achieve metallic bonding. In this configuration, they are called monolithic fuels. Since in the fabrication process, mainly in the rolling of the fuel plates, temperature is needed to ensure metallurgical stability, formation of new compounds can be observed [2]. For example, it was observed that, for the U-Mo-Al system, compounds of  $(\gamma\text{UMo})\text{Al}_x$ , ( $2 \leq x \leq 4$ ) have some deleterious results over the fuel plate's performance, due to the production of new uranium phases. Most of the new phases have low

thermal conductivity, causing changes in the temperature profiles of the plate, leading to a non-uniform and excessive swelling, among other unwanted effects.

Works have been carried out with the objective of producing more stable and nonreactive fuel phases, as well as more chemically stable matrices. From the results of several experiments carried out over the years, called RERTR experiments, studying UMoX-Al system reactions in diffusion-pairs systems, it was determined that ternary additions of  $X = \text{Zr, Ti or Si}$  to the fuel  $\gamma\text{UMo}$  particles and the addition of Si to the matrix are the most promising candidates for the minimization of the reactions and the formation of the interaction layer. Park et al. [3, 4] showed that under certain experimental conditions, an increase in the content of Zr, Si and Ti minimized the extent of the interaction layer for atomized fuels. However, such ternary elements could promote the  $\gamma\text{-UMo}$  decomposition into  $\alpha\text{-U}$ , a more reactive phase, as a side deleterious effect. Most recently [5], it is shown that, for the usual compositions of 7, 10 and 12 % wt. Mo, the interaction layer is actually formed by 2 to 7 sub layers. The number of sub layers is a function of the molybdenum content.

In terms of the fabrication of  $\gamma\text{UMo}$  alloys and their use as fuels, chemical resistance with the aluminium matrix is only one of the phenomena that must be taken into account, but also the temperatures at which the oxidation reactions starts. The presence of air in the processes of powder fabrication [6], like hydration-dehydration, atomization or machining, will change fuel's particle chemical and physical properties, so does its behavior under irradiation. The definition of the temperature of oxidation as one of the temperature limits of fabrication appears advantageous, to prevent oxidation. Together with the oxidation limit, the temperature with the start of reaction with aluminum is also used as a process temperature limit, mainly in the rolling of the fuel plates. They are also interesting in the verification of possible oxidation reactions occurring during the aluminum experiments.

The main objective of this work is to contribute to the study of the chemical stability of the high density and low enriched  $\gamma\text{-UMo}$  hypoeutectoid alloys fuels, currently being considered to replace the low density ones, such as  $\text{U}_3\text{O}_8$  and the high density silicides  $\text{USi}$ ,  $\text{U}_3\text{Si}_2$  and  $\text{U}_3\text{Si}$ . For this to be accomplished, it is presented and discussed an alternative approach, to the study of the reactions of the formation of the interaction U-Mo-Al layers by means of solid state diffusion-pairs, based on thermal analysis.

It is given here an emphasis on the results of the technique of differential thermal analysis (DTA) and on the choice of a convenient parameter for the analysis of stability and definition of a stability criterion. This technique was chosen to perform the studies of the reactions, due to its simplicity and the production of results with high accuracy.

## 2. Experimental procedure

Samples of uranium alloys and aluminum were assembled in alumina crucibles, in the reaction chamber of the thermal analyzer furnace. Thermal cycles, comprising heating and cooling ramps, were utilized to the observation of the melting and solidification points of aluminum and any reaction products, when formed. After a vacuum level of  $10^{-3}$  mbar, tem-

perature was raised at 10°C/min from the room up to 1000°C, and decreased at the same rate. Temperatures and energies of reactions, showed as peaks in the HF curves, were extracted directly from the DTA curves and, when necessary, calculated. A blank consisting of pure aluminum was obtained, to serve as a comparison basis between the reactive and the non-reactive systems.

Analysis of the results was carried out based on the following considerations, given by the examination of the blank curve, and extensive to all the experiments. Differences between the melting points of aluminum and  $\gamma$ UMo alloys are of the order of 600°C. Thus, during the heating ramp of the thermal cycle, the first peak shown in the curves was related to the melting of aluminum. Since the contact area between the solid fuel and liquid aluminum, produced during the thermal cycles, are larger than the presented by the aluminum when it is kept in its porous form, such as in the compacts, an increase in the probability of the reaction between Al and  $\gamma$ UMo is expected. If a reaction occurs, the corresponding peaks must to appear, indicating release or absorption of heat, after the melting peak of aluminum. Since the mass of the system could be considered as a conserved quantity, due to the slight differences observed between the initial and final masses during the experiments, reaction indicates the formation of phases other than the original ones, usually having different thermal properties, when compared to the reactants. In previous papers, it was determined that, when a ternary UMoAl compound is formed, its stability is strongly dependent on its composition, some of them originating amorphous phases, with bad performance under irradiation.

To check for the changes in the composition of the original or reactant system, a careful examination of the cooling curve was also carried out. On the cooling ramp, the area under the peak corresponding to the aluminum solidification depends on the extent of the reaction of aluminum consumption in the heating step of the cycle. If no aluminum is consumed, indicating that no reaction occurred, it is expected the 1:1 proportion between the cooling (solidification) and heating (melting) areas under the peaks, as shown by the curve of the pure aluminum.

Some possible criteria for the stability of the alloys under aluminum, based on the experimental observations above, were devised, through a comparison between the energies given by the areas enclosed by both peaks, in the melting and solidification parts of the thermal cycle heat flow curves, obtained for each alloy and normalized for the reactant masses. Low cooling / heating ratios indicate low aluminum available for solidification, due to reaction and formation of a stable compound. To verify the possible oxidation of the samples, a comparison between the visual states of the samples, from the reactions with aluminum and oxygen, was made after the end of the thermal cycles. Also, it was made a comparison between the curves for aluminum and oxidation experiments.

Experiments for the stability studies in oxidizing atmosphere were carried out with the same thermal cycles used in the aluminum compatibility experiments. Two classes of samples were analyzed, the as cast and the thermally treated ones. Samples of the  $\gamma$ UMo alloys (5 to 10% wt. Mo) were produced for the oxidation-DTA experiments. Synthetic air (80% nitrogen and 20% oxygen) was introduced into the furnace chamber to guarantee the continuous supply of oxygen during experiments.

The curves of heat flow (HF), mass and temperature, as a function of time, were obtained, and the strategy adopted was to simply register the points on the heat flow curves when the reaction with air started, as given by the DTA equipment. In addition, to compare the effects on stability, promoted by the homogenization treatments, a curve comparing the differences between the starting and maximum points for each composition was constructed, enabling us to derive some conclusions regarding gamma stability under oxygen. Normalization of the curves were carried out to the determination of the areas, the curves shown above are the original ones, given during the experiments.

Based on the experimental data, the next step was the construction of the stability curves. They are curves relating the area under some of the events defining a phenomena, for example, solidification and melting of aluminum peaks and possible reactions for the  $\gamma$ UMo-Al systems, and temperatures of the starting of the reaction, in the case of the  $\gamma$ UMo-O<sub>2</sub> systems, as a function of the composition  $x$  of the gamma  $\gamma$ -U <sub>$x$</sub> Mo alloys. The determination of the extremes (maxima or minima) of the curves, and the analysis of their surroundings, indicates a range of optimal composition, for the improvement of the  $\gamma$ -U <sub>$x$</sub> Mo alloys fuel properties in terms of fabrication and during reactor operation.

Analysis presented here was based on the curves given by the DTA equipment, and the phenomenology relating to the presence of the peaks, due to oxidation reactions, impurities, exothermic or endothermic reactions, changes of the physical states of the system, and the effects of other contaminants are being carried out.

### 3. Results and discussions

#### 3.1. Aluminum

The first graph shows the results of the blank experiment, carried out for the same heating and cooling cycles, having as “reactant” only pure aluminum. It was observed the ratio between the areas under the solidification and melting events was 1:1.12, almost 1:1, indicating the conservation of the aluminum mass in the system, respecting our experimental errors, during the thermal cycle, and also indicating no interference in the experimental results due to aluminum mass loss.

Figures 2 to 5 shows the experimental heat flow curves obtained for each alloy composition, together with the thermal cycle, the curve in red. Points depicted in Figure 2 are called events associated with the phenomena, related to the stability analysis. They are shown in Tables 1 to 3, and described below, the symbol \* refers to data for the as cast sample. The events are: A: first peak, before the start of the aluminum melting; B: start of the melting; C: endothermic heat flow peak for the melting; D: minimum, ending the melting process; E: start of a reaction between uranium alloy and aluminum; F: exothermic peak of reaction; G: end of the reaction; H: another transformation (reaction) peak; I: start of the physical transformation of some new compound formed; J: exothermic peak of the transformation; L: end of the transformation; M: solidification of aluminum starts; N: exothermic peak of the solidification, and O: end of the solidification.

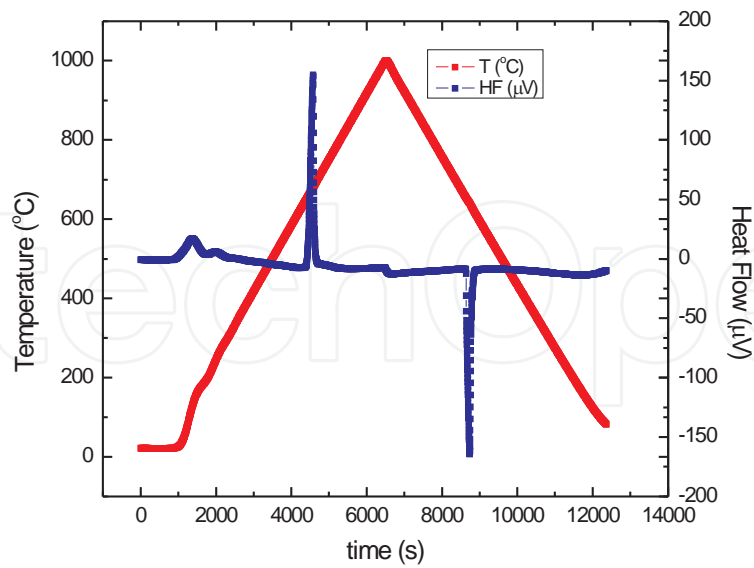


**Figure 1.** Heat flow and thermal cycle curves for pure aluminum [7].

To describe a specific phenomenon, it is suggested the following, based on the events taken as points in the HF curves, and according to the above description. A phenomenon like melting, solidification, etc., defines a set of coordinates given by the events. For example, the pure aluminium melting phenomenon is defined by the events B, C and D. From the data of table 1, their coordinates are B = (4429; 654.54; 0.38), C = (4580; 678.87; 154.78) and D = (4663; 694.12; -0.21).

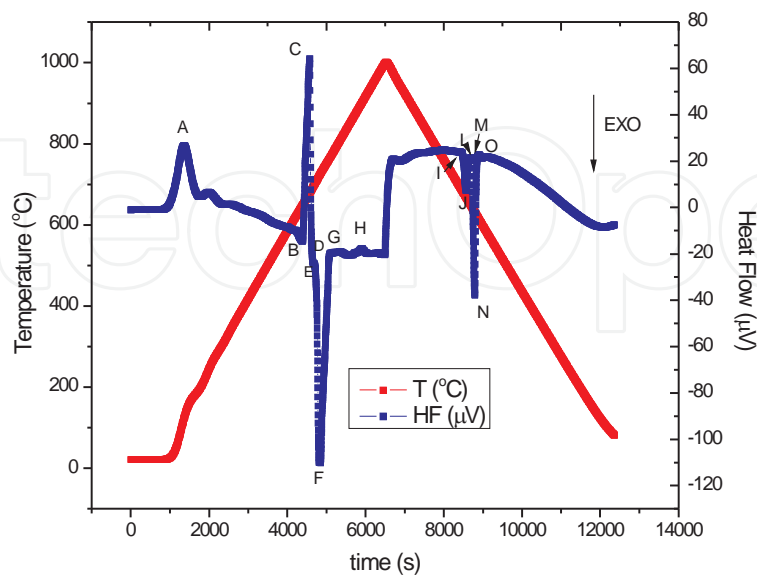


**Figure 2.** Heat flow curve for  $\gamma$ U5Mo, with the events and related phenomena [7].

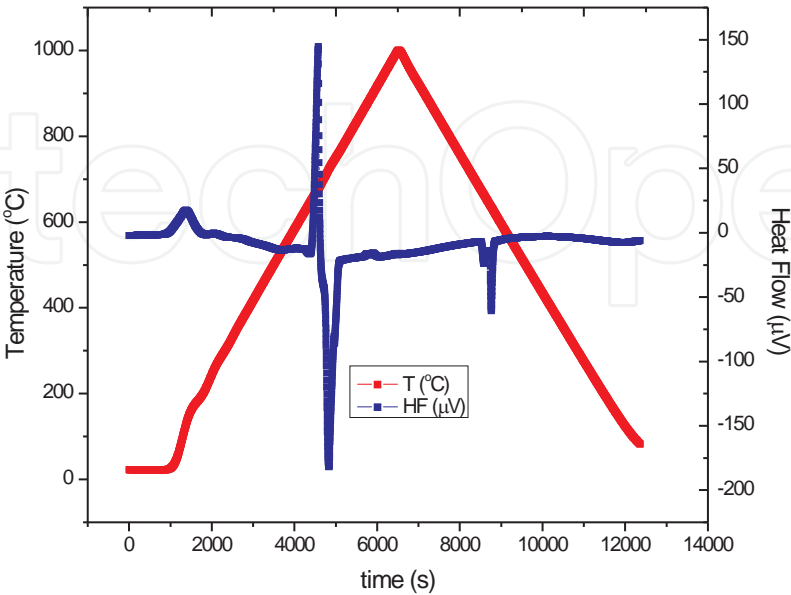


**Figure 3.** Heat flow for  $\gamma$ U6Mo, homogenized 1000°C [7].

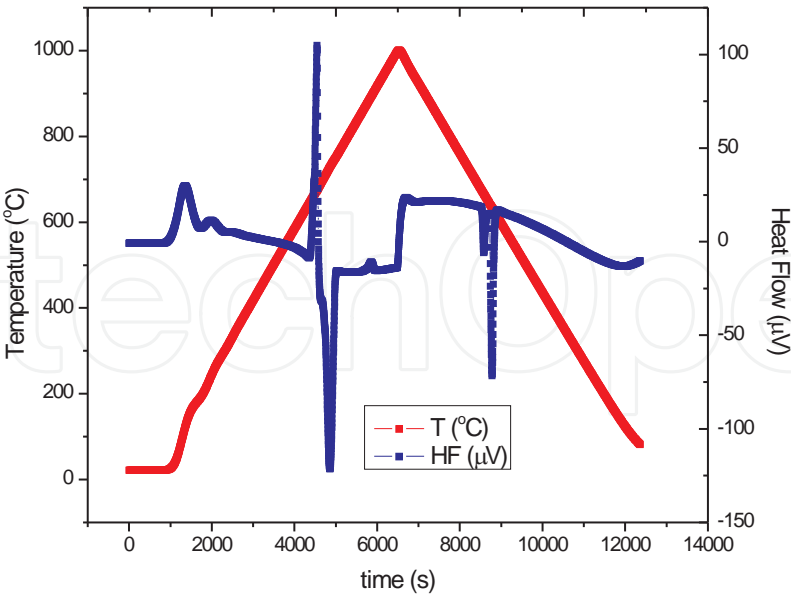


**Figure 4.** Heat flow for  $\gamma$ U6Mo, as cast [7].

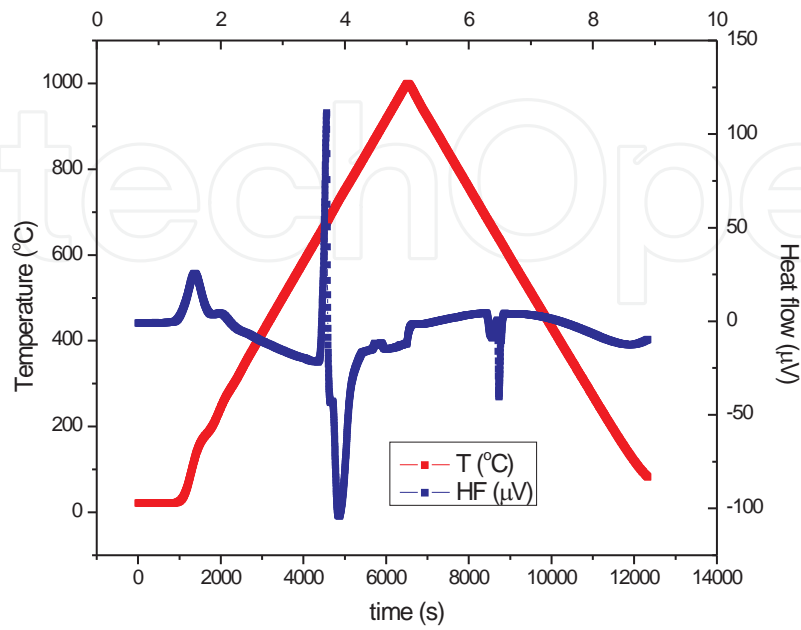


**Figure 5.** Heat flow for  $\gamma$ U7Mo, homogenized 1000°C [7].

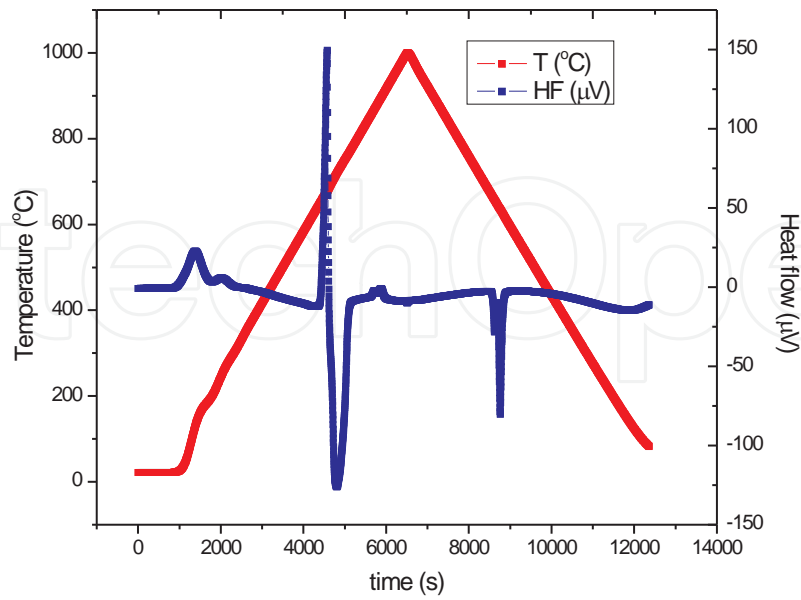


**Figure 6.** Heat flow for  $\gamma$ U8Mo, homogenized 1000°C [7].

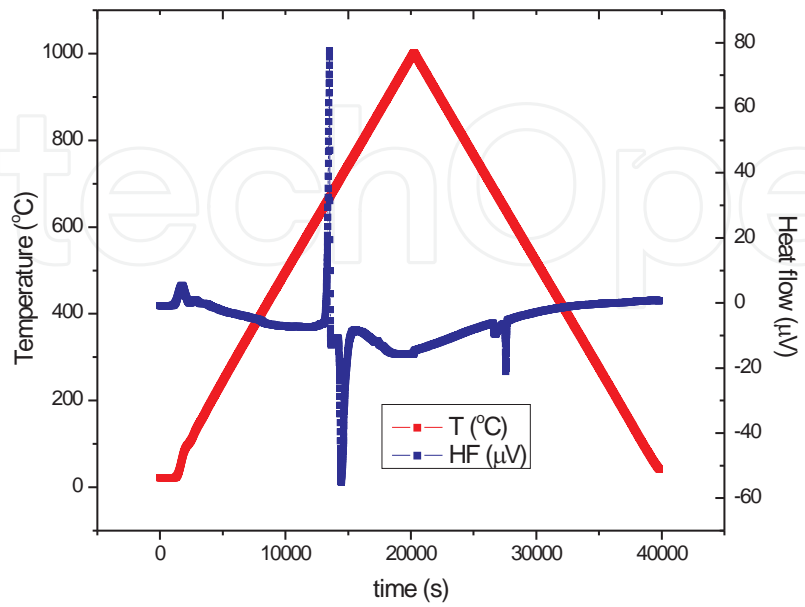


Figure 7. Heat flow curve for  $\gamma$ U9Mo, homogenized 1000°C [7].

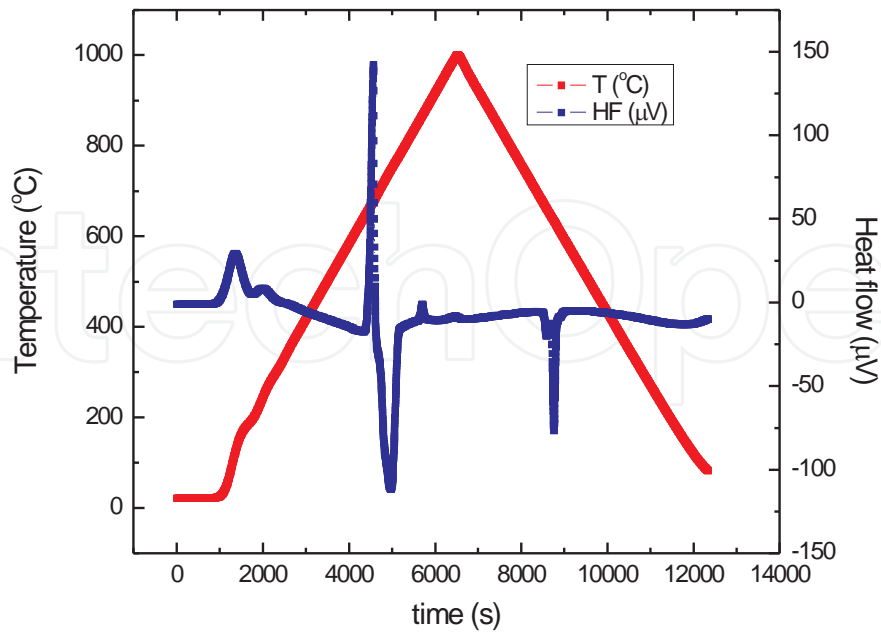


Figure 8. Heat flow curve for  $\gamma$ U10Mo, homogenized 1000°C [7].

First assessment of the values of temperature, heat flow and times, for each of the points, are given in the Tables 1 to 3. Examination shows the evolution of peaks during heating and cooling, after the melting and before the solidification peaks, indicating regions for the formation of the reaction products. Visual examination of the samples showed no changes in their volumes, against the observed and expected volume changes in the oxidation experiments.

Event	$\gamma$ U5Mo	$\gamma$ U6Mo*	$\gamma$ U6Mo	$\gamma$ U7Mo	$\gamma$ U8Mo	$\gamma$ U10Mo	Al°
A	1358	1343	1365	1370	1385	1358	1370
B	4380	4355	4365	4350	4428	4353	4429
C	4570	4548	4575	4558	4573	4565	4580
D	-----	-----	-----	4665	-----	-----	4663
E	4690	4653	4690	4695	4613	4653	-----
F	4848	4858	4833	4868	4808	4970	-----
G	5074	5040	5075	5438	5125	5158	-----
H	5903	5855	5895	5735	5873	5700	-----
I	8498	8525	8493	8405	8525	8470	-----
J	8570	8578	8583	8568	8625	8590	-----
L	8700	8725	8658	8695	8705	8703	-----
M	8700	8725	8658	8695	8705	8703	8638
N	8790	8778	8763	8730	8760	8758	8738
O	8871	8918	8853	8870	8918	8835	8898

**Table 1.** Times (s) for the experimental events [7].

It was stated [8] that reactions of  $\gamma$ UMo alloys with aluminum started typically at the temperature of 645°C. In Figure 1, it was indicated a temperature of 641°C for the melting point of the aluminum, and, as can be viewed in Figures 2 to 8, it is suggested that chemical reaction started soon after the melting phenomena. Thus, it is confirmed the validity of the fundamental assumptions of our approach, to the detection of possible reactions in the U-Mo-Al system. The formation of a layer of liquid aluminum in contact with the  $\gamma$ UMo particles promotes an effective contact between both surfaces, enhancing the probability of reaction.

The entries of the Table 1 are the times of the occurrence of each event for each of the DTA experiments shown in the figures above. They were shown because of their importance in the calculus of the total heat released or absorbed in the system, which defines our stability parameter.

The entries of the Table 2 are the respective temperatures, and the entries of the Table 3 are the respective heat flows. In the following discussions and data analysis, it could be helpful

to made the association  $X \rightarrow (t; T; \Phi)$ , where  $X$  = event, given by the A, B, C, etc., and the triple  $(t; T; \Phi)$  giving its coordinates in the three-dimensional space comprised by the experiments. If no reaction occurs, peaks D and E are coincident, no F peak will appear. In this case, D defines aluminum transformation, and E defines a reaction in the system.

From the data listed in Tables 1, 2 and 3, it is possible to calculate the areas under the peaks, to the determination of the total heat released or absorbed on the system. These results are listed in the Table 4.

The areas were calculated by the determination of the areas below a peak of a set of events. For an example, a triangle basis gives the total time of the phenomena, and the heights are the maximum heat flows. For the purposes of the stability analysis, values of the areas were taken as positive. However, negative signs are still shown, to emphasize the thermodynamical nature of the phenomena, endothermic or exothermic.

Event	$\gamma\text{U5Mo}$	$\gamma\text{U6Mo}^*$	$\gamma\text{U6Mo}$	$\gamma\text{U7Mo}$	$\gamma\text{U8Mo}$	$\gamma\text{U10Mo}$	Al°
A	123.32	117.6	124.31	125.88	130.64	123.31	126.24
B	647.54	643.77	644.14	643.22	654.69	643.19	654.54
C	678.15	674.42	678.86	674.5	676.85	676.48	678.87
D	-----	-----	-----	694.12	-----	-----	694.12
E	699.35	693.2	697.85	699.13	684.16	692.71	-----
F	726.92	728.75	723.76	729.2	719.69	747.24	-----
G	762.68	757.62	762.38	822.39	720.77	777.12	-----
H	901.02	893.09	898.95	871.4	894.95	866.97	-----
I	678.93	674.78	678.22	690.58	672.98	680.48	-----
J	667.3	666.39	663.75	664.36	656.88	661.06	-----
L	646.0	642.24	651.53	643.49	643.76	642.79	-----
M	646.0	642.24	651.53	643.49	643.76	642.79	654.62
N	631.96	634.48	634.48	638.15	635.48	634.52	612.32
O	615.99	611.08	619.74	615.07	609.19	621.53	640.27

**Table 2.** Temperatures (°C) for the experimental events [7].

For the reaction phenomena H, clearly shown in the figures with the exception of  $\gamma\text{U8Mo}$  and  $\gamma\text{U10Mo}$  alloys, it was difficult to define a complete phenomenon in terms of events. The region around this point is being analyzed, and the results will be presented in a future work, together with a more accurate interpretation of the peaks, based on thermodynamical and chemical consideration.

The studies of the reactions in the system U-Mo-Al are important in nuclear technology, since the formation of a stable layer of an insulating material is deleterious to the fuel's per-

formance. Earlier works, like the previously mentioned in the introduction, determined the composition of this layer as a ternary of (UMo)Al<sub>3</sub> and (UMo)Al<sub>4</sub>. However, most recent and accurate works [5] determined that the layer is a combination of at least 2 to 7 sublayers, each having specific composition. According to Perez et al [5], for an UMo alloy with 7 wt% Mo, it was determined for the sublayer near aluminum of UMo<sub>2</sub>Al<sub>20</sub>, UAl<sub>4</sub> and UAl. For the second sublayer, UMo<sub>2</sub>Al<sub>20</sub> and UAl<sub>4</sub>, and up to the pure  $\gamma$ -U7Mo, the layers are composed by UMo<sub>2</sub>Al<sub>20</sub>, UAl<sub>4</sub> and UAl<sub>3</sub>, UMo<sub>2</sub>Al<sub>20</sub> and UAl<sub>3</sub>, U<sub>6</sub>Mo<sub>4</sub>Al<sub>43</sub>, UMo<sub>2</sub>Al<sub>20</sub> and UAl<sub>3</sub>, U<sub>6</sub>Mo<sub>4</sub>Al<sub>43</sub> and UAl<sub>3</sub>, and finally U<sub>6</sub>Mo<sub>4</sub>Al<sub>43</sub> and  $\gamma$ -U. For an alloy of  $\gamma$ -U10Mo, 3 sublayers appeared, UMo<sub>2</sub>Al<sub>20</sub> plus UAl<sub>4</sub>, U<sub>6</sub>Mo<sub>4</sub>Al<sub>43</sub>, UMo<sub>2</sub>Al<sub>20</sub> and UAl<sub>3</sub>, and the nearest from the fuel phase the composition is U<sub>6</sub>Mo<sub>4</sub>Al<sub>43</sub>, UAl<sub>3</sub> and  $\gamma$ -U. This set of materials have different properties under irradiation, for example, U<sub>6</sub>Mo<sub>4</sub>Al<sub>43</sub> transforms to an amorphous structure at less than 1 damage per atom (dpa) and, at 100 dpa, presenting a high density of voids, which is related to possible sites for bubble nucleation in their structure. The presence of the ternary phases from the U-Mo-Al is responsible for the poor irradiation performance of the fuels, under irradiation conditions.

Evento	$\gamma$ U5Mo	$\gamma$ U6Mo*	$\gamma$ U6Mo	$\gamma$ U7Mo	$\gamma$ U8Mo	$\gamma$ U10Mo	Al°
A	26.71	29.92	17.41	25.55	22.71	29.19	16.86
B	-14.56	-8.59	-16.31	-21.6	-0.04	-17.31	0.38
C	64.31	104.87	144.76	111.51	149.6	142.04	154.78
D	-----	-----	-----	-43.44	-----	-----	-0.21
E	-24.28	-31.35	-39.38	-42.68	-1.24	-27.23	-----
F	-110.15	-121.39	-181.82	-103.98	-126.05	-111.52	-----
G	-21.14	-15.42	-24.06	-16.48	-11.01	-17.14	-----
H	-17.64	-10.9	-15.78	-11.8	-0.9	-1.19	-----
I	20.65	17.98	-6.66	4.4	-2.66	-5.68	-----
J	7.34	-5.76	-23.96	-8.86	-28.34	-20	-----
L	21.46	15.08	-14.8	0.64	-9.65	-12.58	-----
M	21.46	15.08	-14.8	0.64	-9.65	-12.58	-8.63
N	-37.81	-71.68	-60.61	-40.36	-80.25	-76.43	-164.3
O	22.8	16.99	-6.72	4.31	-3.08	-10.48	-9.42

**Table 3.** Heat flows ( $\mu$ V) for the experimental events [7]

To solve this problem, it is studied in the RERTR experiments ternary additions to the  $\gamma$ -UMo alloys and also additions in the matrix, and the elements considered as promising are Zr, Ti, and Si. It is a convenient approach to keep the layer stable, since fuel properties and performance can be estimated with accuracy.  $\gamma$ -U7Mo and  $\gamma$ -U10Mo are the most studied for this purpose.

Event / $m_i / E_i$	U5Mo	$\gamma$ U6Mo*	$\gamma$ U6Mo	$\gamma$ U7Mo	$\gamma$ U8Mo	$\gamma$ U10Mo	Al°
$m_t$	149.144	148.909	168.991	173.298	175.507	155.642	
$m_c$	75.836	73.94	89.5	97.437	91.654	77.095	
$m_{Al}$	73.308	74.692	79.491	75.86	83.853	78.546	82.010
BCD(E)							
$E_t$	174.04	249.83	331.96	261.11	158.37	316.71	
$E_c$	342.27	503.14	626.79	464.40	303.25	639.38	
$E_{Al}$	354.07	498.07	701.75	596.49	331.47	627.57	441.89
Area	25.9	37.2	56.1	45.3	27.8	49.3	36.2
D(E)FG							
$E_t$	225.13	254.72	341.96	318.98	349.87	289.87	
$E_c$	442.76	512.98	645.68	567.33	669.96	585.21	
$E_{Al}$	458.03	507.82	722.89	728.70	732.28	574.39	
Area	-33.6	-37.9	-57.8	-55.3	-61.4	-45.1	---
H (Area)	-17.64	-10.9	-15.78	-11.8	-0.9	-1.19	
IJL(M)							
$E_t$	74.38	30.21	13.27	19.04	22.76	16.27	
$E_c$	36.55	60.83	25.05	33.87	43.58	32.85	
$E_{Al}$	37.80	60.22	28.05	43.50	47.63	32.25	
Area	-2.7	-4.5	-2.2	-3.3	-3.9	-2.5	---
L(M)NO							
$E_t$	68.71	113.69	57.52	42.79	89.66	54.35	
$E_c$	135.13	228.97	108.61	76.12	171.69	109.73	
$E_{Al}$	139.79	226.66	121.60	97.77	187.67	107.71	492.35
Area	-10.3	-16.9	-9.7	-7.5	-15.7	-8.5	-40.4

Table 4. Areas (mV.s), reduced for the samples masses [7].

However, it was shown by our results that there is a strong tendency for reactions in all the compositions, evidenced by the events and phenomena from the curves. One of the ways to support the above arguments is due to the evaluation of the differences in the areas above the solidification and melting peaks of the aluminum, shown in Figures 2 to 8. From the blank experiment, it was obtained an area ratio of 1.12, which was not kept constant in the U-Mo-Al system experiments. Thus, some amount of aluminum was consumed, probably by the reactions D(E)FG and H, as is shown in the heating ramps. During cooling, free aluminum solidifies, producing a less intense N peak. The difference allows us to estimate masses for the products and other quantitative parameters, together with the analysis of the IJL(M) phenomena.

In the first column of the Table 4, Event corresponds to the set of coordinates of a phenomenon, defined by the letters A, B, C, etc.;  $m_i$  is the masses considered for the analysis, for the calculations,  $i = c$  for the fuel,  $i = Al$  for the aluminum, and  $i = t$  for the total mass, the sum of  $m_i$  and  $m_c$ . They appear in the first three lines of data. A row starting with  $E_i$ ,  $i = c$ ,  $Al$  or  $t$ , presents the normalization results for the respective masses. Since we are analyzing the behavior of the aluminum peaks and with aluminum, rows of interest are labeled with  $E_{Al}$ .

Data listed in Table 4 were obtained from Tables 1 to 3, and used to build the stability curve, presented on Figure 6. It can be noted that  $\gamma$ U9Mo alloy data is not listed. It was detected a possible misinterpretation of the data during the software data process for this specific alloy. So, it is not included in the stability analysis graphic. A detailed verification is in progress, however will not be presented in the present article.

Phenomena like BCDE, DEFG, H, IJLM, LMNO and others that can be derived from the complete analysis of the heat flow or gain of mass curves, can all be studied for stability considerations. To exemplify, next figure is constructed considering the exothermic reaction peaks resulting from the DEFG phenomena, for each alloy.

From Figure 9 it is possible to observe that there is a tendency for the production of more exothermic reactions with aluminum when we consider compositions of 7 to 8%wt Mo. In terms of stability, it indicates that, if a reaction of the formation of the interaction layer is going to occur during fabrication or during reactor operation, compounds formed are probably more stable than those formed in the extremes of the composition.

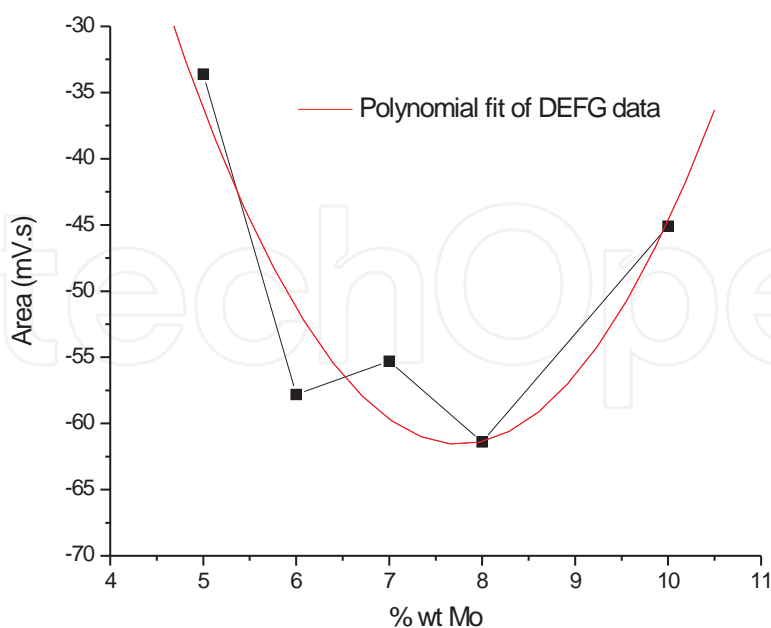


**Figure 9.** Results from the phenomenon DEFG.

Since the interaction layer formation is a phenomenon with high probability of occurrence, due to the temperatures involved during fabrication, irradiation conditions, etc., formation of such stable compounds are favoured.

Also from Figure 9, it is indicated that more stable compounds are formed in the region between 7 to 8% wt. Mo. The second-degree polynomial fit indicates the composition of 7.701% as a minimum, thus as the most stable one. This result is confirmed by the analysis of the results of the oxidation experiments, explained in the following item.

### 3.2. Oxygen or oxidizing atmosphere

The results of the differential thermal analysis for the  $\gamma$ UMo alloys are presented below, Figures 10 to 21, showing the curves of mass gain, thermal cycle and heat flow. For each system, it was determined the temperatures where oxidation occurs, with the total mass gain after the experiments.

Since, during the fabrication of the fuel plates, we are interested in the temperature where chemical reactions start, first assessment of stability criteria was defined in terms of the maximum temperatures and the starting temperature of oxidation. Since a parabolic behavior is obtained, if we analyze the temperature differences between the as cast and thermally treated samples, it was stated as a possible second criterion, which takes into account the differences in microstructure for each class of samples.

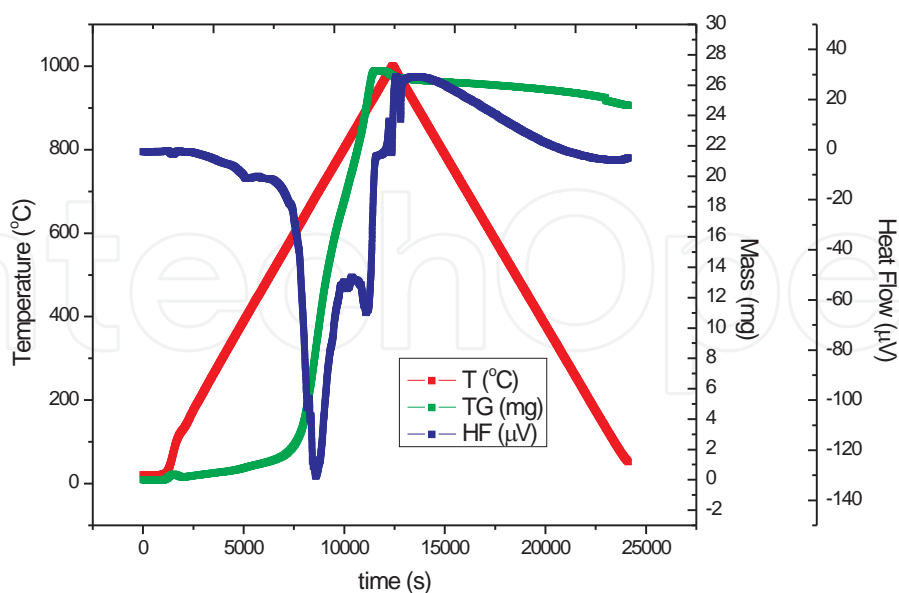


**Figure 10.** Curves of heat flow and mass gain,  $\gamma$ U5Mo, homogenized 1000°C [7].

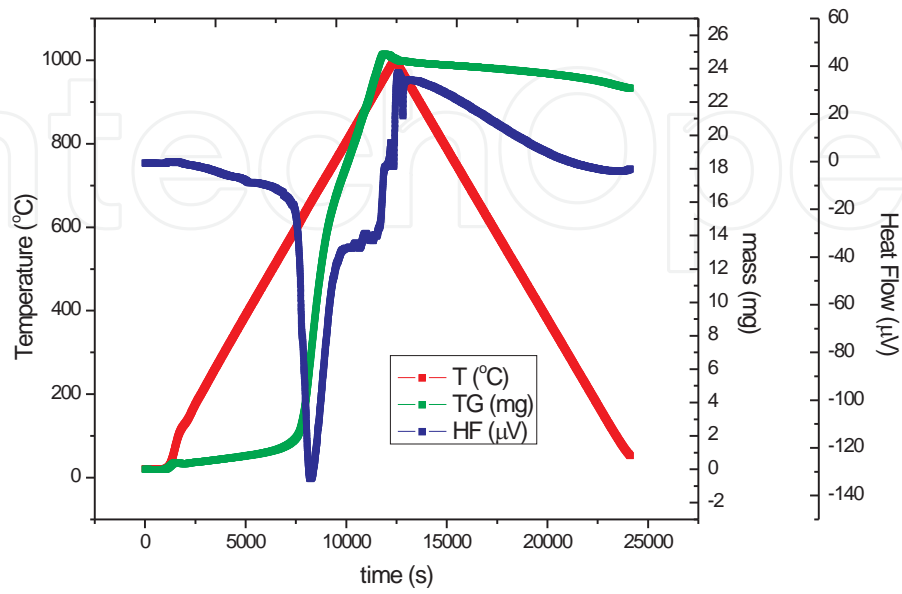


**Figure 11.** Curves of heat flow and mass gain,  $\gamma$ U5Mo, as cast [7].

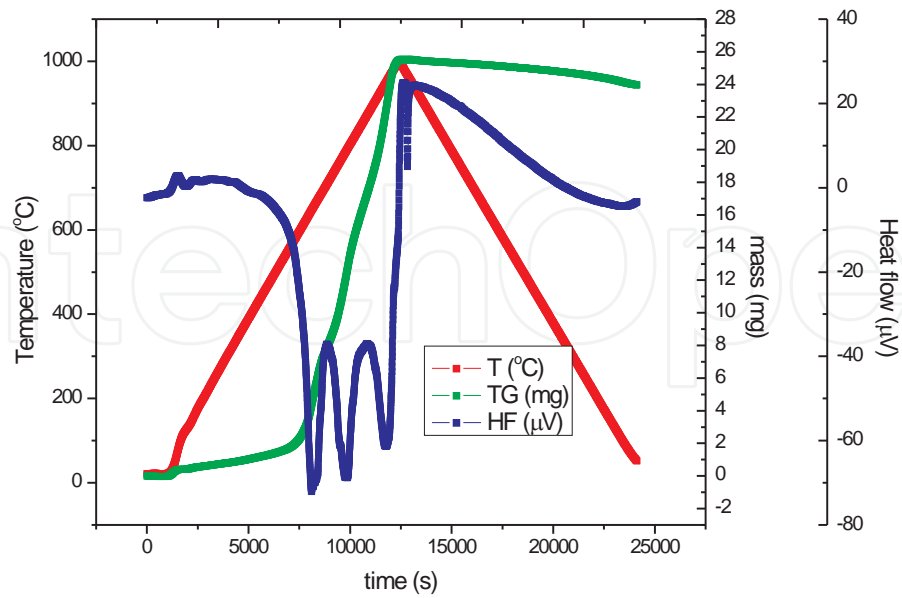


**Figure 12.** Curves of heat flow and mass gain,  $\gamma$ U6Mo, homogenized 1000°C [7].

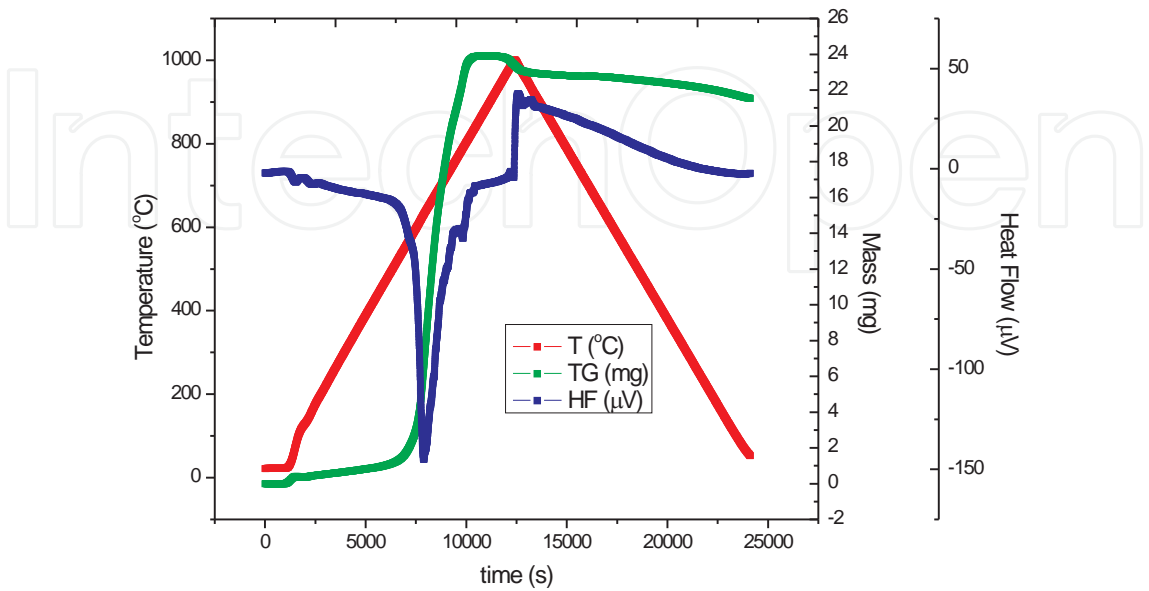


**Figure 13.** Curves of heat flow and mass gain,  $\gamma$ U6Mo, as cast [7].

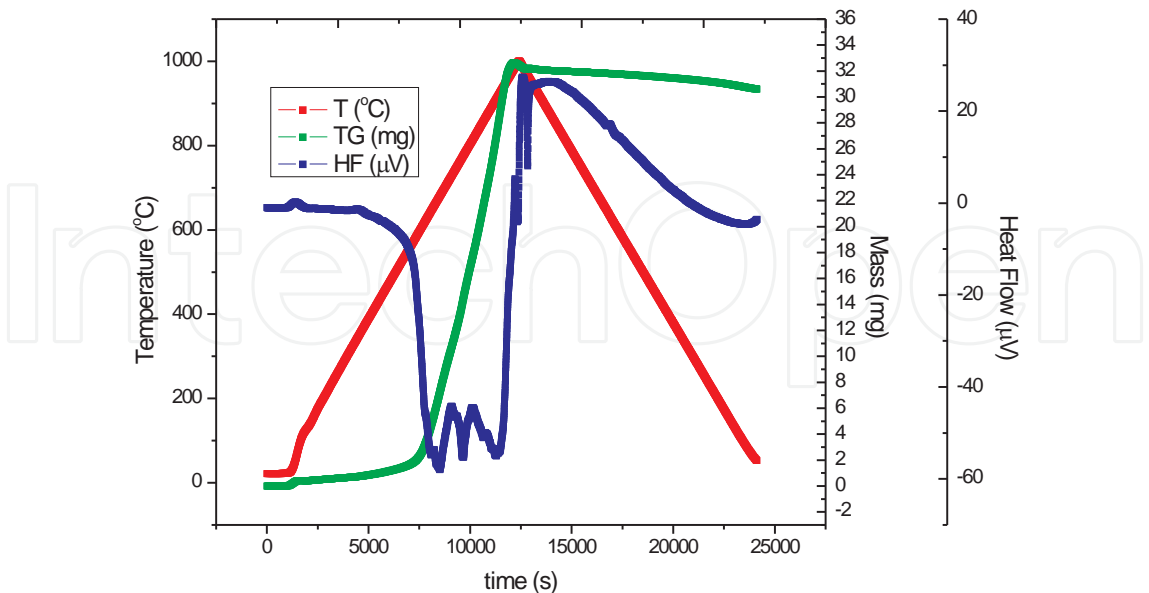


**Figure 14.** Curves of heat flow and mass gain,  $\gamma$ U7Mo, homogenized 1000°C [7].

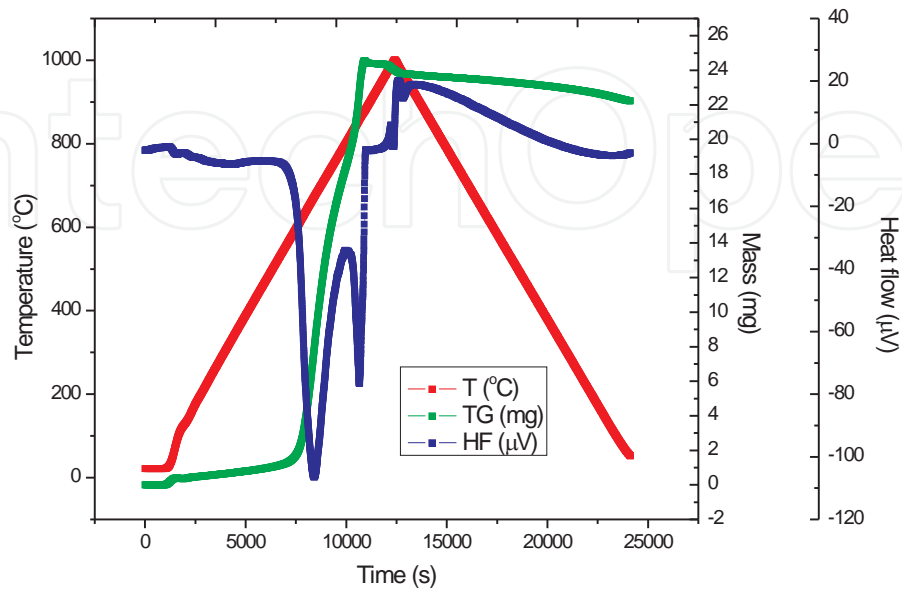


**Figure 15.** Curves of heat flow and mass gain,  $\gamma$ U7Mo, as cast [7].

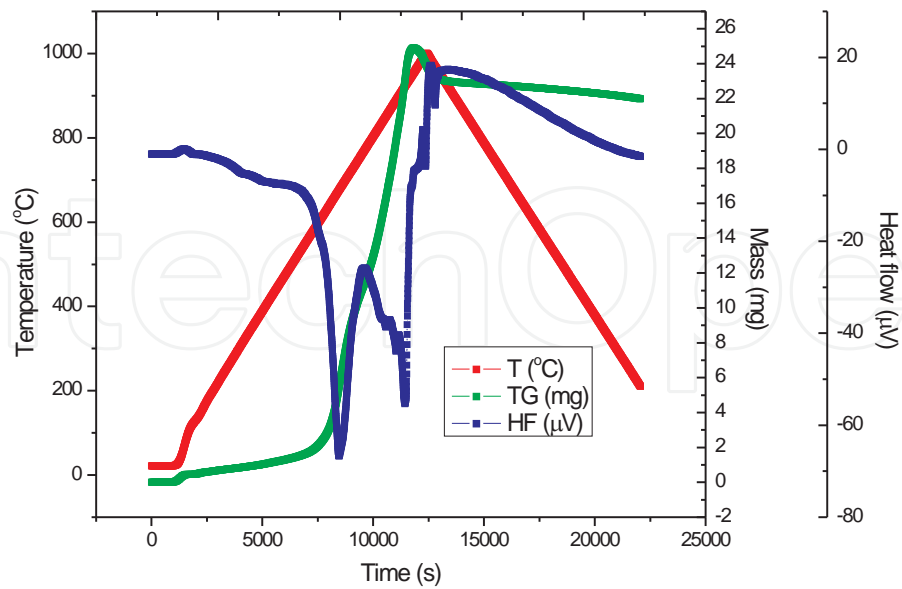


**Figure 16.** Curves of heat flow and mass gain,  $\gamma$ U8Mo, homogenized 1000 $^{\circ}\text{C}$  [7].

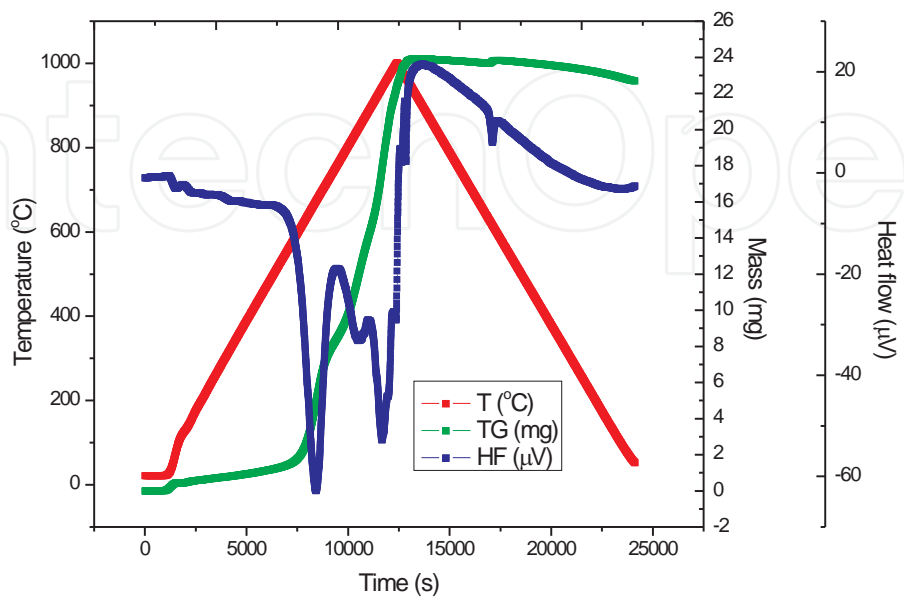


Figure 17. Curves of heat flow and mass gain,  $\gamma$ U8Mo, as cast [7].

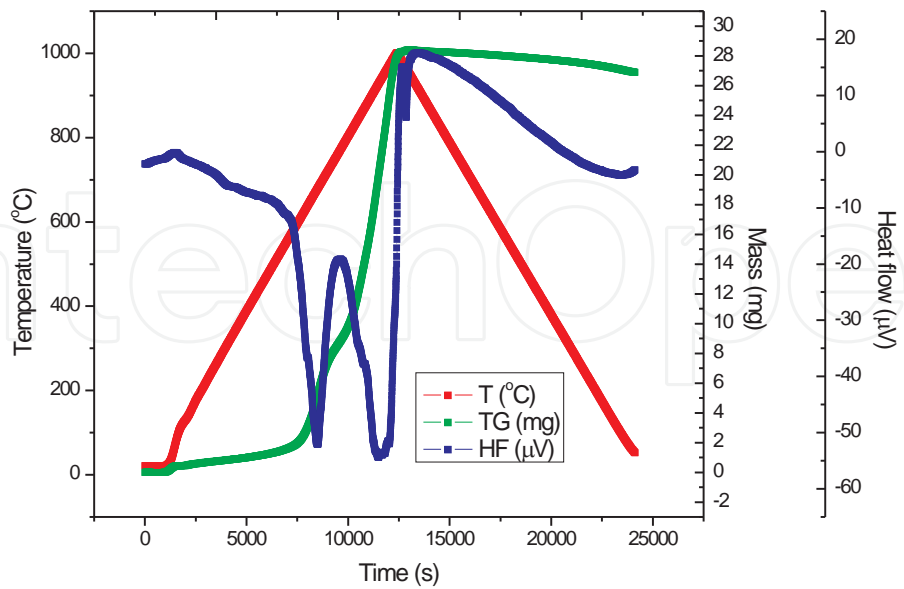
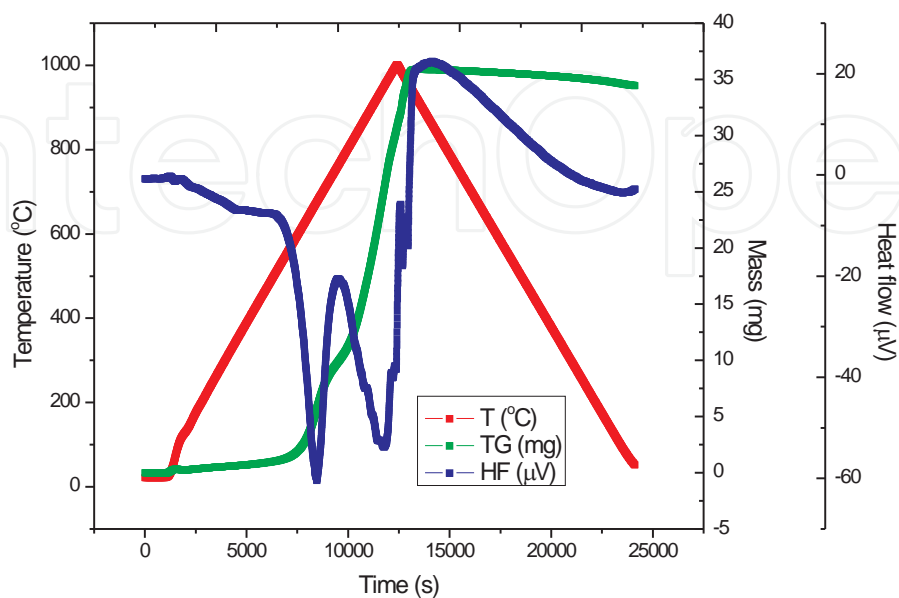
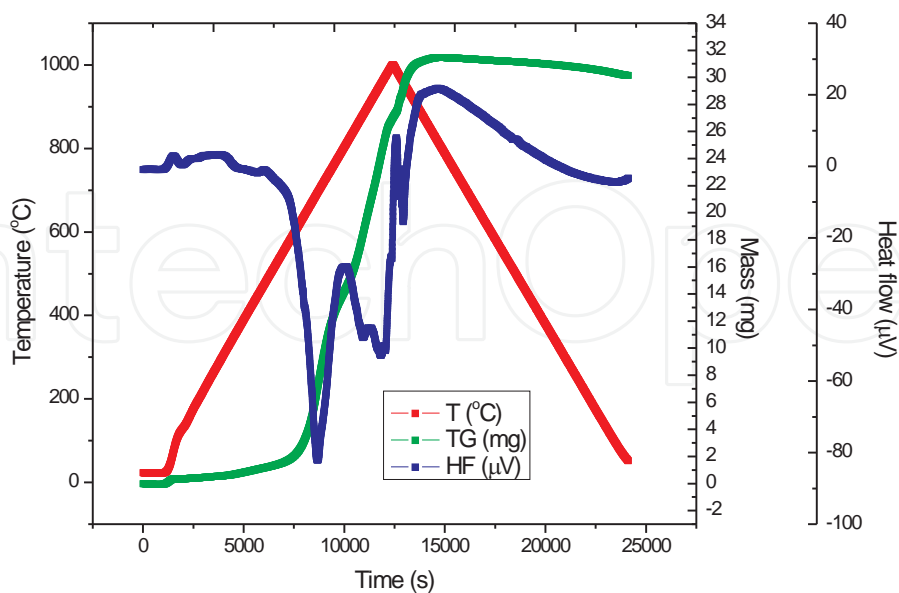


Figure 18. Curves of heat flow and mass gain,  $\gamma$ U9Mo, homogenized 1,000°C [7].



**Figure 19.** Curves of heat flow and mass gain,  $\gamma$ U9Mo, as cast [7].



**Figure 20.** Curves of heat flow and mass gain,  $\gamma$ U10Mo, homogenized 1000°C [7].

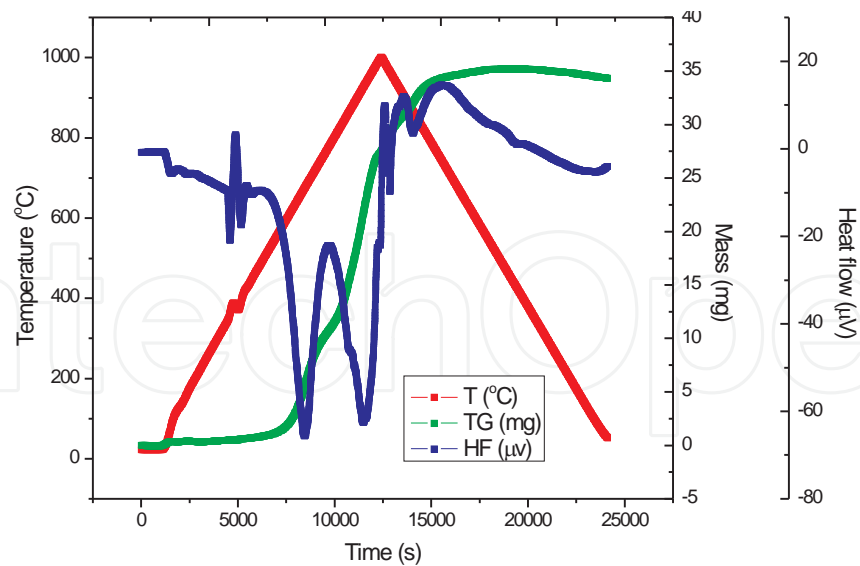


**Figure 21.** Curves of heat flow and mass gain,  $\gamma$ U10Mo, as cast [7].

The temperatures of the start and maximum of oxidation are presented in Table 5 and shown graphically in the Figure 22. The choice for the first peak is mandatory for fabrication purposes, since it indicates a maximum of temperature to avoid oxidation of the fuel in an oxygen-rich environment.

The results shows that thermally treated alloys are more resistant to the oxidation than the as cast ones, and this resistance slightly increases with the increase in Mo content, showing a discontinuity for the case of the 6%wt, Figure 22. The abnormal behavior of the  $\gamma$ U6Mo alloy is possibly due to several factors, like its more refined grain structure, some impurity that acted as inoculants, or even to a more pronounced Mo segregation, which possibly was not reduced with thermal treatments. This abnormal behavior was also observed during irradiation, in the first RERTR tests [1], and some authors suggest that at this percentage another kind of mechanism of alpha precipitation, instead of the gamma to alpha conversion, occurs.

Alloy composition	as cast		thermally treated	
	Start temperature (°C)	Maximum temperature (°C)	Start temperature (°C)	Maximum temperature (°C)
$\gamma$ U5Mo	549.70	660.31	581.35	687.55
$\gamma$ U6Mo	517.80	630.67	536.26	646.75
$\gamma$ U7Mo	542.21	672.36	553.29	680.34
$\gamma$ U8Mo	545.10	672.57	558.84	676.30
$\gamma$ U9Mo	535.25	675.82	565.35	679.73
$\gamma$ U10Mo	526.03	675.03	577.15	694.16

**Table 5.** Main temperature events, for the  $\gamma$ UMo compositions tested [7]

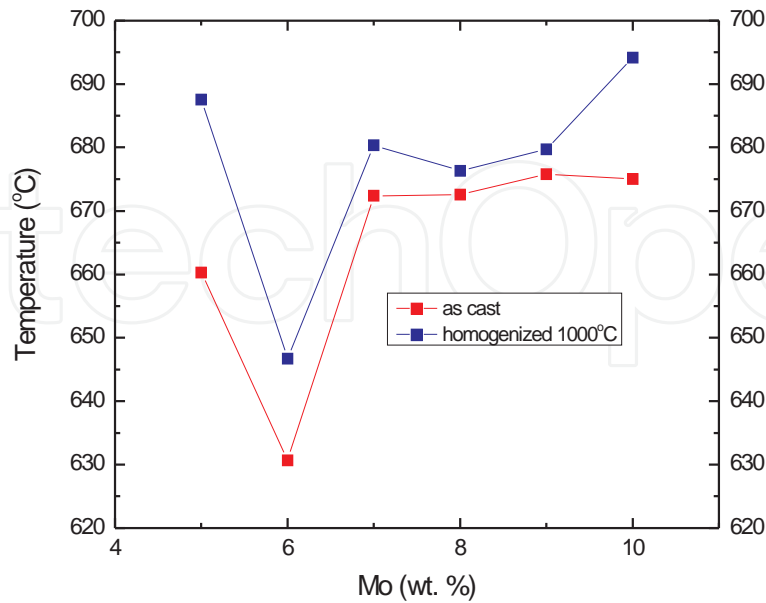


**Figure 22.** Temperatures of the first DTA peaks,  $\gamma$ -UMo alloys.

Instead of defining a peak or starting temperature as a stability criterion, it was found more accurate to state one which is related to the alloy's microstructure. This stability criterion is based on the determination of the curves of the differences in oxidation temperatures between the as cast and thermally treated samples, for each of the Mo contents, at the maximum and start temperatures. The respective graphics are shown below.

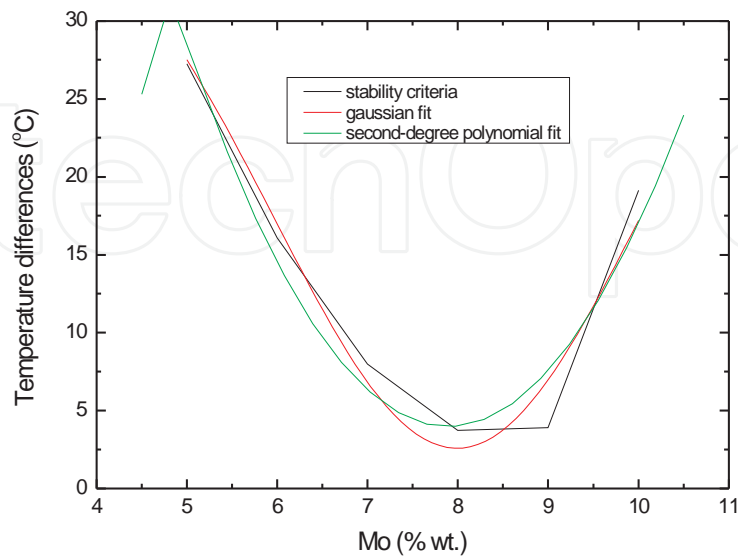


**Figure 23.** Oxidation temperature differences at maximum [7].

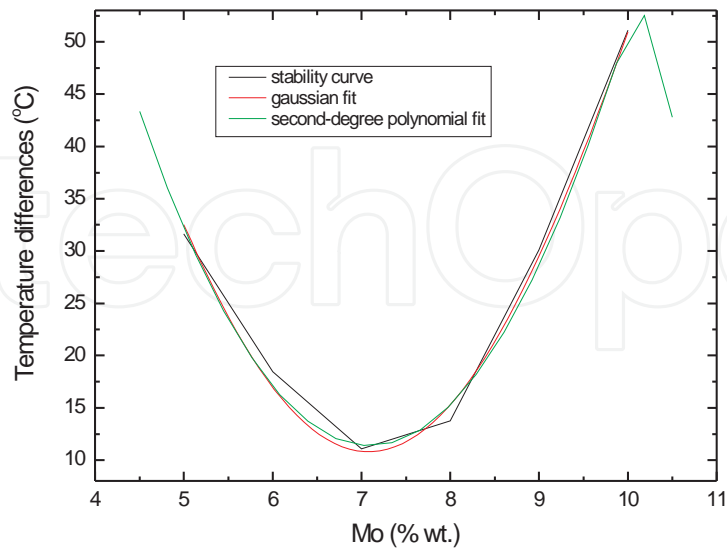


**Figure 24.** Oxidation temperature differences at start [7].

Comparing the microstructures of the as cast and thermally treated alloys, it is observed that high amounts of alpha phase are presented in the low Mo (5 to 6% wt) alloys, decreasing with the increase in the Mo content. On the other side, porosity increases with the Mo additions, as shown in the curves for alloy’s density as a function of composition, see [7]. Since diffusion of oxygen is enhanced by the presence of porosities, and the reactive characteristic of the samples are characterized by the presence of the alpha phase, it is expected for the stability curve to have an extreme. Oxygen diffusion through the samples could be improved when the Mo content is at the extremes of composition. In the intermediate composition ranges there is neither enough alpha nor porosity to react with oxygen, leading to the behavior shown in Figures 23 and 24.

The point of minimum in both curves indicates whether the effect of the thermal treatments is minimal on these compositions. For the reactions with air, the point of minimum is at the value of 7.079 (54) %wt of molybdenum, for the curves of start of oxidation temperatures, while for the curve of maxima, the point of minimum was at 7.990 (147) %wt of molybdenum. For the ease of visualization, a second degree polynomial fit was applied to the curves. The minimum obtained is at 7.094 and 7.894 %wt of molybdenum, and the equations are:

$$\Delta T = 250.4587 - 67.403\%Mo + 4.7507 \left(\%Mo\right)^2 \tag{1}$$

and:

$$\Delta T = 187.5971 - 46.5249\%Mo + 2.4968 \left(\%Mo\right)^2 \tag{2}$$

Through the use of the differential operator  $[d / d(\%Mo)]$  over the  $\Delta T = f(\%Mo)$  curve, the minima mentioned above were obtained after  $[d\Delta T / d(\%Mo)] = 0$ , since we are searching for % of Mo addition values for the optimal stabilization of the UMo alloys.

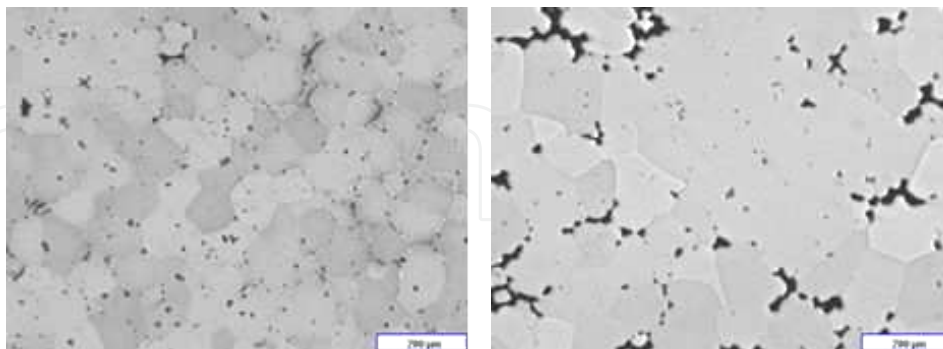


**Figure 25.** Micrographies of  $\gamma$ UMo alloys, 5% wt. Mo (left) and 10%wt. Mo (right) [7].

In other words, the behavior of the temperature differences for the maximum and starting oxidation for a given %wt molybdenum concentration parameter, is explained by the fact that a thermal treatment applied to a stable alloy will not produce a remarkable effect in terms of changes in the oxidation process, if the alloy has a stable structure. So, the differences in the oxidation temperatures are at a minimum value for such compositions.

Also, the analysis performed for this set of experiments confirms the results of the experiments with aluminum, enabling the use of the temperature differences as a parameter for the evaluation of the stability of the alloys.

## 4. Conclusions

One of the main problems with  $\gamma$ UMo for the use as fuels in research reactors is its reaction with the Al matrix. Additions of ternary elements have been considered to keep the fuel integrity in terms of its chemical and physical properties, during fabrication and irradiation. In the present work, the choice was for the analysis of the behavior of the binary  $\gamma$ UMo alloys, in conditions near of the possible chemical environments found in the fabrication and under irradiation. Instead of the study of the effect of ternary additions in the stabilization of the alloys, it is also convenient to study the stability of the binary alloys, in order to set an optimal interval of Mo additions. It is suggested here the use of a differential thermal analysis to provide, based on the definition of some stability criteria, an alternative way to assess the alloys who promotes optimal properties.

The Gaussian or parabolic behavior can also be related to the alloy's stability. As explained above, hypoeutectoid  $\gamma$ UMo alloys can be viewed, according to its compositions, as having remarkable different properties. When related to its behavior in the presence of the alpha phase, whose content decreases with the addition of Mo, or in terms of density, since porosi-

ty tends to increase with an increase in Mo percentage, stability results are very different. Thus it is natural to suppose that there will be an extreme in the stability parameter, adopted here as the difference in oxidation temperatures between the as cast and thermally treated samples for the same %wt. Mo. The minimum is shown in compositions of 7 to 8%wt. Mo, where the systems achieve optimal conditions in terms of stability, when thermal treatments produces minimal effects in the performance of the fuels under oxidation.

On the other hand, their behavior in the presence of aluminum shows an extreme near the same compositions of the oxidation experiments, also leading to the conclusion that between seven and eight percent of Mo we can obtain more stable alloys. The thermodynamics and possible mechanism of stabilization, and the parabolic and Gaussian behavior of the results, are objects of our current studies.

The results agreed with the choice of the composition of 7% wt. Mo for the fabrication of  $\gamma$ UMo fuels and its use in research reactors. The data presented here is supported by previous results, regarding UMo fuel reactions with aluminium. Thus, it was shown that the DTA experiments carried out in this work, together with the definition of a suitable stability parameter, can be used as an alternative way to the analysis of the stability of the  $\gamma$ -UMo systems, for use as fuels in nuclear research reactors.

## Author details

Fábio Branco Vaz de Oliveira and Delvonei Alves de Andrade

Nuclear and Engineering Center, Nuclear and Energy Research Institute, Brazilian Nuclear and Energy National Commission, IPEN-CNEN/SP, Cidade Universitária, São Paulo, SP, Brazil

## References

- [1] Meyer MK, et al. Irradiation Behavior of Uranium-Molybdenum Dispersion Fuel: Fuel Performance Data from RERTR-1 and RERTR-2, Proceedings of the XXII RERTR Meeting, Budapest, Hungary, 1999.
- [2] Varela CLK, et al. Identification of Phases in the Interaction Layer Between U-Mo-Zr / Al and U-Mo-Zr / Al-Si. Proceedings of the XXIX RERTR Meeting, Prague, Czech Republic, 2007.
- [3] Park JM, et al. Interdiffusion Behaviors of U-Mo-Zr / Al-Si. Proceedings of the XXVIII RERTR Meeting, Cape Town, South Africa, 2006.
- [4] Park JM, et al. Interdiffusion Behaviors of U-Mo-Ti / Al-Si, Proceedings of the XXIX RERTR Meeting, Prague, Czech Republic, 2007.

- [5] Perez E., Keiser Jr. DD, Sohn YH. Metallurgical and Materials Transactions A, vol. 42A, October 2011, pp. 3071-3083.
- [6] Pasqualini EE. Advances and Perspectives in U-Mo Monolithic and Dispersed Fuels. Proceedings of the XXVIII International Meeting on Reduced Enrichment of Research Reactors, Cape Town, South Africa, 2006.
- [7] Oliveira FBV. Development of a High Density Fuel Based on Uranium-Molybdenum Alloy with High Compatibility in High Temperatures. PhD thesis, University of São Paulo, 2008.
- [8] Kim YS, et al. Interaction-Layer Growth Correlation for (U-Mo) / Al and Si added (U-Mo) / al Dispersion Fuels. Proceedings of the XXVIII RERTR Meeting, Cape Town, South Africa, 2006.
- [9] Oliveira FBV, et al. Thermal and Chemical Stability of Some Hypoeutectoid  $\gamma$ UMo Alloys. Proceedings of the 12<sup>th</sup> Research Reactor Fuel Management RRFM, Hamburg, Germany, 2008.

